Small cationic antimicrobial peptides delocalize peripheral membrane proteins

Michaela Wenzel[a], Alina Iulia Chiriac[b], Andreas Otto[c], Dagmar Zweytick[d], Caroline May[e], Catherine Schumacher[f], Ronald Gust[g], H. Bauke Albada[h], Maya Penkova[h], Ute Krämer[i], Ralf Erdmann[j], Nils Metzler-Nolte[h], Suzana K. Straus[k], Erhard Bremer[l], Dörte Becher[c], Heike Brötz-Oesterhelt[f], Hans-Georg Sahl[b], and Julia Elisabeth Bandow[a,1]

[a]Biology of Microorganisms, [h]Bioinorganic Chemistry, and [i]Plant Physiology, [e]Immune Proteomics, Medical Proteome Center, and [j]Institute of Physiological Chemistry, Ruhr University Bochum, 44801 Bochum, Germany; [b]Institute for Medical Microbiology, Immunology, and Parasitology, Pharmaceutical Microbiology Section, University of Bonn, 53113 Bonn, Germany; [c]Department of Microbial Physiology and Molecular Biology, Ernst Moritz Arndt University, 17489 Greifswald, Germany; [d]Biophysics Division, Institute of Molecular Biosciences, University of Graz, 8010 Graz, Austria; [f]Institute for Pharmaceutical Biology and Biotechnology, Heinrich Heine University, 40225 Düsseldorf, Germany; [g]Department of Pharmaceutical Chemistry, University of Innsbruck, 6020 Innsbruck, Austria; [k]Department of Chemistry, University of British Columbia, Vancouver, BC, Canada V6T 1Z1; and [l]Department of Biology, University of Marburg, 35037 Marburg, Germany

Edited by Michael Zasloff, Georgetown University Medical Center, Washington, DC, and accepted by the Editorial Board February 27, 2014 (received for review October 22, 2013)

Short antimicrobial peptides rich in arginine (R) and tryptophan (W) interact with membranes. To learn how this interaction leads to bacterial death, we characterized the effects of the minimal pharmacophore RWRWRW-NH_2. A ruthenium-substituted derivative of this peptide localized to the membrane in vivo, and the peptide also integrated readily into mixed phospholipid bilayers that resemble Gram-positive membranes. Proteome and Western blot analyses showed that integration of the peptide caused delocalization of peripheral membrane proteins essential for respiration and cell-wall biosynthesis, limiting cellular energy and undermining cell-wall integrity. This delocalization phenomenon also was observed with the cyclic peptide gramicidin S, indicating the generality of the mechanism. Exogenous glutamate increases tolerance to the peptide, indicating that osmotic destabilization also contributes to antibacterial efficacy. *Bacillus subtilis* responds to peptide stress by releasing osmoprotective amino acids, in part via mechanosensitive channels. This response is triggered by membrane-targeting bacteriolytic peptides of different structural classes as well as by hypoosmotic conditions.

mechanism of action | respiratory chain | hypoosmotic stress response | metallocenes

During the past two decades, bacterial antibiotic resistance has grown into a major threat to public health, restoring infectious diseases to the list of leading causes of death worldwide (www.who.int/healthinfo/statistics/bodgbddeathdalyestimates.xls). As a reaction to this health crisis, several efforts currently are underway to discover and develop new natural and synthetic antibiotic compounds. One promising antibiotic class is antimicrobial peptides, which occur naturally as part of host defense systems in all domains of life (1–4). Antimicrobial peptides range in length from four to more than 100 amino acids and fall into a number of different structural classes, including α-helical amphiphiles, lipopeptides, glycopeptides, lantibiotics, and short cationic peptides.

The short cationic peptides offer a potent alternative to longer natural antimicrobial peptides. The latter can be difficult to isolate and are complicated to synthesize chemically, but short cationic peptides are generated readily by solid-phase peptide synthesis and are easily accessible for chemical derivatization (5–8). They are characterized by positively charged and by hydrophobic amino acids (9, 10). Previous mechanistic studies in vitro have examined the interactions of the peptides with membranes or membrane extracts (11–15), but their effects on bacterial physiology have been largely underexplored.

A more complete understanding of how these short cationic antimicrobial peptides bring about bacterial cell death is needed to further their optimization and development for practical applications. To achieve this understanding, we studied the synthetic hexapeptide RWRWRW-NH_2 (referred to hereafter as "MP196") (see *SI Appendix*, Fig. S1 for structure) as a model representing the minimal pharmacophore of positively charged and hydrophobic amino acids (16, 17). It is effective against Gram-positive bacteria including methicillin-resistant *Staphylococcus aureus* strains, is moderately effective against Gram-negative bacteria, has low toxicity against human cell lines, and displays low hemolytic activity (18). MP196 therefore is a promising lead structure for derivatization and already has yielded peptides with improved activities and altered pharmacological properties (19). For example, in a recent systematic L-to-D exchange scan peptides with significantly reduced hemolytic activity could be identified (20).

Proteomic profiling of the Gram-positive bacterium *Bacillus subtilis* exposed to MP196 provided a starting point for mechanistic

Significance

Multidrug-resistant bacteria present an acute problem to medicine, generating interest in novel antimicrobial strategies. Antimicrobial peptides currently are being investigated, both as antibiotics and as immunomodulatory agents. Many antimicrobial peptides interact with the bacterial membrane, a previously underexplored antibiotic target. We present a system-based study of the mode of action of small cationic peptides and the mechanisms that bacteria use to defend against them. We show that peptide integration into the membrane causes delocalization of essential peripheral membrane proteins. This delocalization impacts on two cellular processes, namely respiration and cell-wall biosynthesis. We describe a bacterial survival strategy in which mechanosensitive channels in the bacterial membrane establish osmoprotection against membrane-targeting bacteriolytic peptides. Understanding the peptides' mode of action and bacterial survival strategies opens up new avenues for devising peptide-based antibacterial strategies.

Author contributions: M.W., H.-G.S., and J.E.B. designed research; M.W., A.I.C., A.O., D.Z., C.M., C.S., and R.G. performed research; H.B.A., M.P., U.K., N.M.-N., S.K.S., E.B., D.B., and H.B.-O. contributed new reagents/analytic tools; M.W., A.I.C., A.O., D.Z., C.M., C.S., R.G., R.E., H.B.-O., and J.E.B. analyzed data; and M.W., H.B.-O., H.-G.S., and J.E.B. wrote the paper.

The authors declare no conflict of interest.

This article is a PNAS Direct Submission. M.Z. is a guest editor invited by the Editorial Board.

Data deposition: The mass spectrometry proteomics data have been deposited to the ProteomeXchange Consortium (http://proteomecentral.proteomexchange.org) via the PRIDE partner repository [Vizcaino JA, et al. (2013) The Proteomics Identifications (PRIDE) database and associated tools: Status in 2013. *Nucleic Acids Res* 41(D1):D1063–D1069]. The dataset ID is PXD000181.

[1]To whom correspondence should be addressed. E-mail: julia.bandow@rub.de.

This article contains supporting information online at www.pnas.org/lookup/suppl/doi:10.1073/pnas.1319900111/-/DCSupplemental.

studies. It identified two major areas for analysis: membrane and cell-wall integrity and energy metabolism. The proteome analysis prompted further investigation into the deregulation of amino acid biosynthesis, which revealed that *B. subtilis* counteracts the attack on the cell envelope by triggering an osmoprotective release of glutamate.

Results

Inhibition of Macromolecule Biosynthesis Points to the Bacterial Cell Envelope as a Target of MP196. To explore the inhibition of macromolecule biosynthesis by MP196 in vivo, we studied incorporation of radioactive precursors. Cells were exposed to MP196 concentrations that reduced growth rates by ~50% unless noted otherwise (*SI Appendix*, Fig. S2). MP196 moderately inhibited incorporation of DNA, RNA, protein, and cell-wall precursors (Fig. 1*A* and *SI Appendix*, Fig. S3). To separate the primary event from secondary effects, the activation of reporter genes was studied in *B. subtilis* (Fig. 1*B*). Each of the reporter strains had been shown previously to respond specifically to the inhibition of a particular cellular process using different antibiotics (21). MP196 did not activate transcription from promoters of *yorB*, *helD*, or *bmrC*, which are indicative of DNA damage, RNA synthesis inhibition, and translation inhibition, respectively. The *liaI* promoter, which is responsive to inhibition of steps in membrane-bound cell-wall biosynthesis, was activated weakly, whereas *ypuA*, which is responsive to both membrane-associated and membrane-independent cell-wall stress, was strongly activated.

The Proteomic Response of *B. subtilis* Provides Additional Evidence That MP196 Targets the Cell Envelope. The response of *B. subtilis* to treatment with MP196 was studied at the proteome level by combining 2D gel-based and LC-MS–based approaches (*SI Appendix, Results of the Comparative Proteome Analysis* and Tables S1–S4). Proteins indicative of general cell-envelope stress, membrane stress, energy limitation, and cell-wall stress were strongly up-regulated upon exposure to MP196 (Fig. 1*C*), indicating that the cell envelope is the primary target of MP196. From a library of proteome response profiles that includes the responses to more than 50 antibiotic agents (22–26), several antibiotics were identified that share subsets of these marker proteins with MP196, all affecting the bacterial cell envelope (*SI Appendix*, Table S5). The strongest overlap in up-regulated proteins was observed for the membrane-targeting agents gramicidin S and valinomycin. Gramicidin S, a member of the small cationic antimicrobial peptide class, is structurally distinct from MP196: It is a cyclic amphipathic peptide that does not contain the arginine or tryptophan residues found in MP196. It disrupts membrane function by integrating into the lipid bilayer (27). Valinomycin is an uncharged dodecadepsipeptide, which acts as a potassium-carrier ionophore. Both antibiotics were selected as close comparators to study the antibiotic mechanism of MP196. We also chose vancomycin and nisin as comparator compounds. They both share marker proteins of cell-envelope stress with MP196. Vancomycin is a lipid II-binding cell-wall biosynthesis inhibitor, and nisin, in addition to inhibiting cell-wall biosynthesis by binding lipid II, forms heteromultimeric membrane pores with lipid II.

A Stereospecific Binding Site Is Not Required for MP196 Target Interaction. Given the proteomics results, it seemed likely that the lipid bilayer is a direct target of the peptide. However, to exclude the possibility that MP196 binds to a protein target and downstream effects elicit the observed proteomic response, we investigated the importance of peptide stereochemistry for antibacterial activity and MP196–target interaction using an all–D-amino acid peptide (D-MP196). D-MP196 was as active as MP196

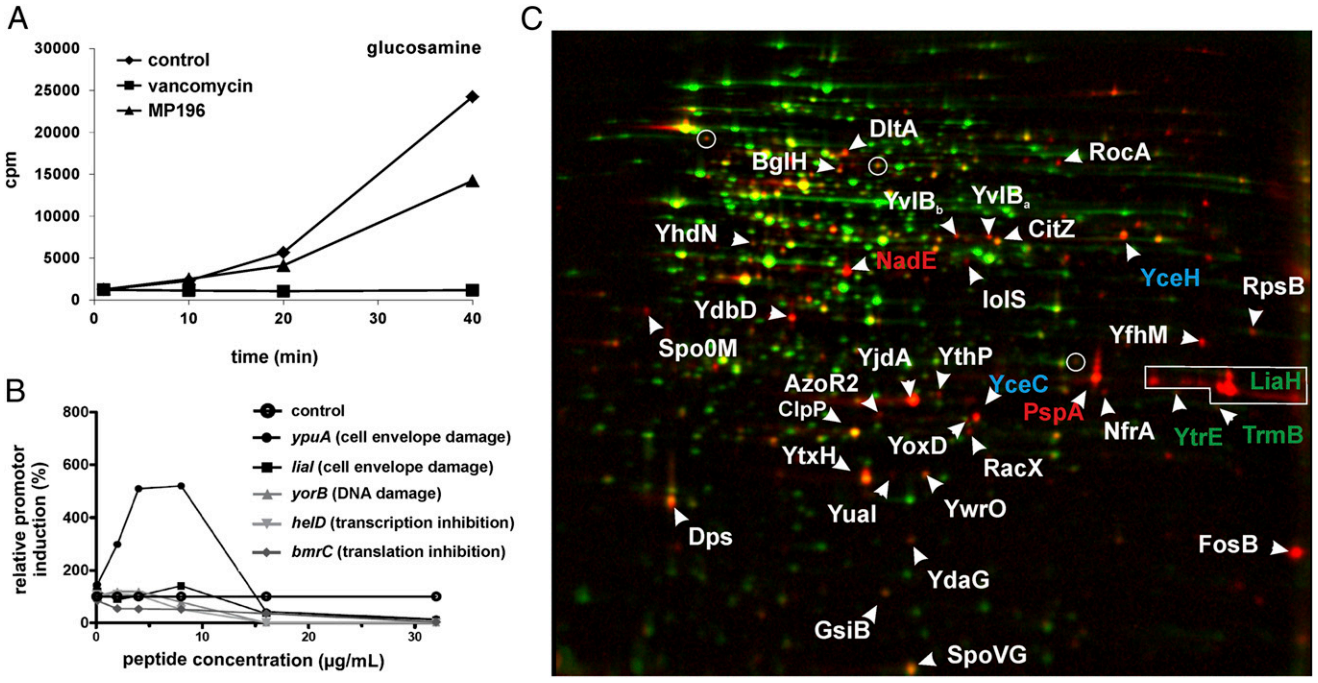

Fig. 1. Narrowing down the target area. (*A*) [^{3}H]-glucosamine incorporation by *S. simulans* upon treatment with MP196 or vancomycin. (*B*) Transcription activation of selected *B. subtilis* promoters indicative of inhibition of specific cellular processes. Cells were incubated with increasing concentrations of MP196 for predetermined times depending on the induction kinetics of the respective reporter strains. (*C*) 2D gel-based proteome analysis of MP196-treated *B. subtilis*. Synthesis rates of cytosolic proteins of MP196-treated (false-colored in red) and untreated (false-colored in green) *B. subtilis* were compared based on [^{35}S]-methionine labeling. In the overlaid autoradiographs, down-regulated proteins appear green, up-regulated proteins appear red, and proteins expressed at equal rates appear yellow. Unidentified proteins are marked by circles. Blue labels indicate marker proteins for general cell-envelope stress, green labels identify cell-wall biosynthesis inhibition, and red labels are markers for membrane stress.

against *B. subtilis* (18), and the two forms had highly similar proteome responses (*SI Appendix*, Fig. S4 *A* and *B*). Thus, stereochemistry is not crucial for target interaction, making it unlikely that MP196 binds to a specific site on a protein target.

MP196 Affects Cell Morphology. The impact of nonlytic concentrations of MP196 and gramicidin S on the morphology of *B. subtilis* cells was examined by transmission electron microscopy (TEM) (Fig. 2*A*). MP196-treated cells displayed characteristic cell-wall lesions. The cell wall at these sites is thinner, suggesting a loss of integrity. Gramicidin S-treated cells did not retain their shape during sample preparation, culminating in the leakage of cell contents and cell collapse. Thus, although both peptides induce similar proteome-response patterns, the structural impairment of the *B. subtilis* cell envelope is more severe after gramicidin S treatment than after MP196 exposure.

MP196 Accumulates in the Bacterial Cell Envelope. To study the subcellular localization of MP196 in vivo, a ruthenocene-substituted derivative Rc-C(O)-WRWRW-NH_2 (MP276) (see *SI Appendix*, Fig. S1 for structure) was synthesized for TEM and atomic absorption spectrometry studies. The ruthenocene substitution did not affect antibacterial activity negatively (18), and ruthenium alone is not toxic.

Thin sections of untreated and MP276-treated *B. subtilis* were prepared omitting the lead-staining step, which is used as contrast agent in electron microscopy (Fig. 2*B*). Accordingly, in the preparations of untreated cells the cell envelope is poorly contrasted compared with the cytosol. However, in MP276-treated cells the cell envelope is seen in high contrast, showing that the peptide with the electron-dense ruthenium label accumulates in the cell envelope.

Peptide Concentrations Are Highest in the Bacterial Membrane. Graphite furnace atomic absorption spectrometry provides absolute quantitation of the ruthenium-labeled peptide in subcellular fractions. Because ruthenium does not occur naturally in bacteria, it is ideally suited for peptide tracing in the cellular environment (28).

The absolute ruthenium amounts were related to the volumes of the cellular compartments to give compartment concentrations (*SI Appendix*, Table S6). Volumes were calculated based on high-resolution cryo-electron microscopy studies of the *B. subtilis* membrane and cell-wall structures (29, 30). The ruthenium concentration in the membrane fraction exceeded concentrations measured in the cytosolic and cell-wall fractions by factors of 15 and 17, respectively. In agreement with peptide tracing by TEM, the principal localization of MP276 is the membrane. During sample preparation, cells were washed with EDTA several times. There was no significant elution of ruthenium ($\sim 10^{-21}$ mol per cell), suggesting strong binding of the peptide to the phospholipid bilayer. Lower but still significant amounts of peptide were detected in the cell wall, which can function as a barrier that detains antibiotics (31). Concentrations of ruthenium above background levels also were detected in the cytosolic fraction, suggesting that the peptide has some ability to cross the lipid bilayer.

MP196 Integrates into Phospholipid Bilayers That Mimic Gram-Positive Membranes but Not Erythrocyte Membranes. Interaction of MP196 with the membrane was investigated by differential scanning calorimetry (DSC) using model membranes consisting of the two most abundant phospholipids in the *B. subtilis* membrane (32), namely 1,2-dipalmitoyl-*sn*-glycero-3-phosphatidylglycerol (DPPG) and 1,2-dipalmitoyl-*sn*-glycero-3-phosphatidylethanolamine (DPPE), in an 88:12 ratio (Fig. 3*A*). DSC monitors the thermotropic-phase behavior of the lipid bilayer. Changes in pattern are indicative of perturbation of the membrane bilayer and packaging of the phospholipids' fatty acyl chains and, therefore, of peptide integration. Deconvolution of

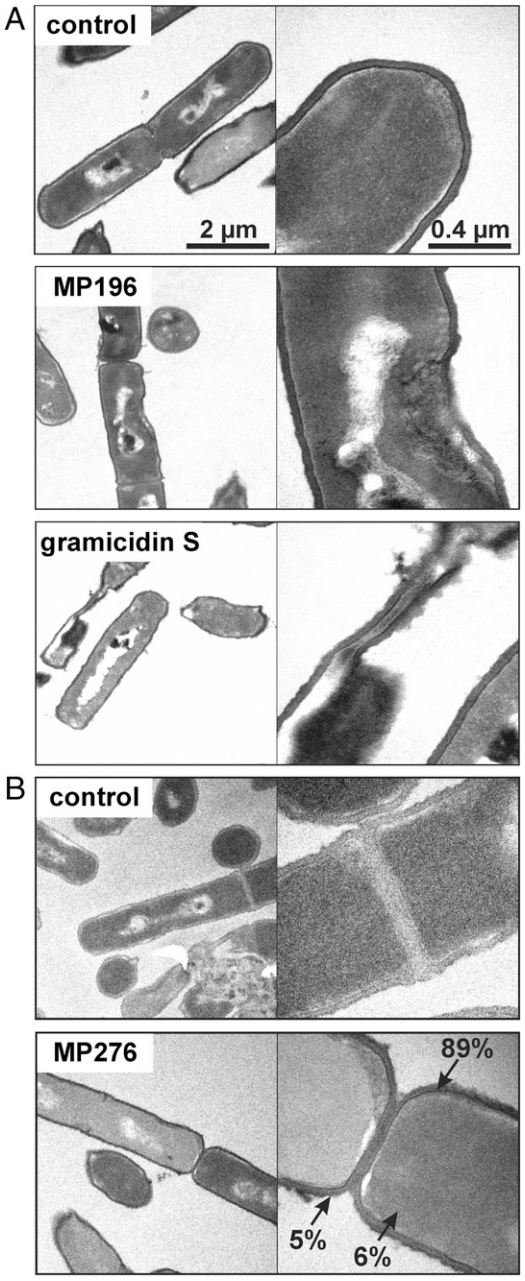

Fig. 2. Peptide effects on cells and subcellular localization. (*A*) TEM images of peptide-treated *B. subtilis*. Cells were fixed with 2% uranyl acetate, and ultrathin sections were stained with 0.2% lead citrate in 0.1 M NaOH. (*B*) In vivo peptide tracing using the ruthenocene-substituted MP196 derivative MP276. *B. subtilis* cells were fixed with 2% uranyl acetate. Sections remained unstained to avoid interference of lead with the ruthenium signal. Ruthenium in the cytosol, membrane, and cell wall was quantified by atomic absorption spectroscopy.

the thermograms indicates that MP196 integrates into the phospholipid bilayer, generating "peptide-affected domains" (14). These are characterized by a broadening of the existing transition and the appearance of a small transition at lower temperatures, reflecting rearrangement of the lipid mixture, and, consequently, alterations in packaging of the lipids at the emerging borderlines.

When bilayers composed of a single type of phospholipid were used, the influence of MP196 was far less pronounced. A broadening of the shoulder at lower temperatures indicated the formation of some peptide-affected domains on DPPG bilayers,

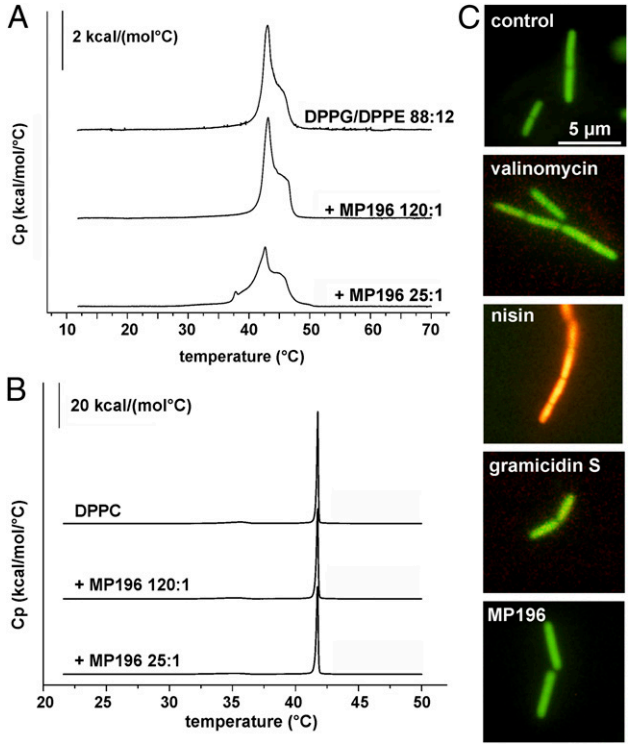

Fig. 3. Interaction with the membrane. (*A*) DSC thermograms of lipid bilayers consisting of 88:12 DPPG/DPPE incubated with MP196. Changes in thermotropic-phase behavior caused by perturbation of fatty acyl packing indicate peptide integration. (*B*) DSC thermograms of lipid bilayers consisting of DPPC. (*C*) Overlaid fluorescence microscopy images of *Bac*-Light-stained *B. subtilis* treated with valinomycin, nisin, gramicidin S, and MP196. A red-fluorescing dye selectively stains cells with large membrane holes; a green-fluorescing dye stains all cells independently of membrane integrity. Cells with intact membranes appear green, and cells with perforated membranes appear orange.

but no effect was seen using pure DPPE (*SI Appendix*, Fig. S5) or pure 1,2-dipalmitoyl-*sn*-glycero-3-phosphatidylcholine (DPPC) (Fig. 3*B*), which typically are used to model erythrocyte membranes (33). That MP196 affected DPPG but not DPPE implies a preference for negatively charged over neutral lipids and could explain the preference for bacterial over erythrocyte membranes. This supposition is consistent with the known low hemolytic activity of MP196 (18). A preference for negatively charged phospholipids has been shown previously for other very small RW-rich peptides, Combi-1 (Ac-RRWWRF-NH_2) and $LfcinB_{4-9}$ (RRWQWR-NH_2), using the same method (reviewed in ref. 13).

Peptide Integration Does Not Lead to Pore Formation. We used fluorescence staining to test whether in vivo integration of the MP196 peptide results in pore formation in *B. subtilis*. The green-fluorescent dye SYTO 9 crosses intact membranes, whereas the red-fluorescent propidium iodide enters bacterial cells through lesions in the membrane (Fig. 3*C*). Pore-forming nisin allowed both dyes to enter *B. subtilis* cells, resulting in orange cells. MP196 treatment, as well as treatment with non–pore-forming gramicidin S and valinomycin, resulted in green-fluorescent cells—like the untreated control—suggesting that MP196 does not act by forming large pores. The same conclusions were drawn from measuring peptide-induced potassium leakage from *Bacillus megaterium* cells into choline buffer (*SI Appendix*, Fig. S6*A*). In contrast to the positive control, nisin, MP196 released little potassium, even at concentrations equivalent to 50 times the minimal inhibitory concentration (MIC).

MP196 Does Not Disturb Metal Cation Homeostasis. The *B. subtilis* proteomic responses to MP196 and to the potassium ionophore valinomycin were markedly similar. To investigate whether MP196 integration into the membrane disturbs metal cation homeostasis, total cellular ion concentrations were determined after peptide treatment in chemically defined culture broth (*SI Appendix*, Fig. S6*B*). In agreement with the observed lack of potassium efflux in choline buffer, no significant decrease in any metal ion was observed after MP196 treatment. In contrast, gramicidin S treatment caused a significant decrease in potassium, magnesium, and manganese levels. Valinomycin-treated cells selectively accumulated potassium (an eightfold increase), probably because of overcompensation. These results fit well with the observation that, despite provoking a strong proteome response, valinomycin does not inhibit *B. subtilis* growth (24).

MP196 Integration Causes Membrane Depolarization. Many membrane-targeting antibiotics, including gramicidin S and valinomycin, depolarize the bacterial membrane (27, 34). Depolarization was investigated using a *B. subtilis* strain carrying a GFP fusion to the cell division-regulating protein MinD. Normally localized at the cell poles and in the cell-division plane, MinD delocalizes upon depolarization, resulting in a spotty pattern of GFP-MinD distribution (35). In contrast to the normal MinD pattern in the untreated control cells, MinD delocalization was seen in MP196 and gramicidin S-treated cells (Fig. 4*A*). Depolarization upon MP196 treatment was confirmed in *B. megaterium* with the voltage-sensitive fluorescent probe $DiSC_35$ (*SI Appendix*, Fig. S6*C*).

ATP Levels Drop in MP196-Treated Cells. Sudden depolarization should result in energy limitation, and energy limitation also would be consistent with the proteome response. Intracellular ATP levels of *B. subtilis*, determined using a luciferase assay, showed a 60% reduction in cellular ATP content in MP196-treated cells and a 70% reduction in gramicidin S-treated cells (Fig. 4*B*), whereas valinomycin and nisin caused 30% drops. Thus, MP196 has a considerable impact on energy metabolism. No significant ion efflux was observed under the test conditions, indicating that depolarization and energy limitation are not caused solely by ion transfer.

MP196 Inhibits the Respiratory Chain at the Cytochrome *c* Level. Because of the lack of pore formation and ion transfer, which are typical causes of a breakdown of energy metabolism, we tested whether components of the respiratory chain are inhibited by MP196. Inhibition of ATP synthase would limit ATP directly. Proton-pumping activity was monitored in *Micrococcus flavus* inverted vesicles using the pH-sensitive probe acridine orange (*SI Appendix*, Fig. S6*D*). The ATP synthase inhibitor lactoferrin (36) served as a positive control. No inhibition of ATP synthase activity was observed at MP196 concentrations corresponding to those used in the proteome analysis.

Inhibition of the respiratory chain upstream of ATP synthase would contribute to the breakdown of the membrane potential, resulting in the loss of ATP synthesis. Using *M. flavus* inverted vesicles, inhibition of the respiratory chain was monitored with iodonitrotetrazolium chloride, a reduction-sensitive dye (Fig. 4*C*). Rotenone and antimycin A, specific inhibitors of complexes I and III of the respiratory chain, respectively, were used as comparator compounds. Rotenone reduced electron transport activity by 20%, and antimycin A did so by 50%. MP196 displayed similar inhibition efficiency, reducing electron transport by 30%. MP196 inhibition was additive with either rotenone or antimycin A, suggesting that MP196 inhibits a different component of the respiratory chain.

Cytochrome *c*, which is located on the outer membrane leaflet, transfers electrons from complex III to complex IV. Its localization after MP196 treatment was investigated by Western blot

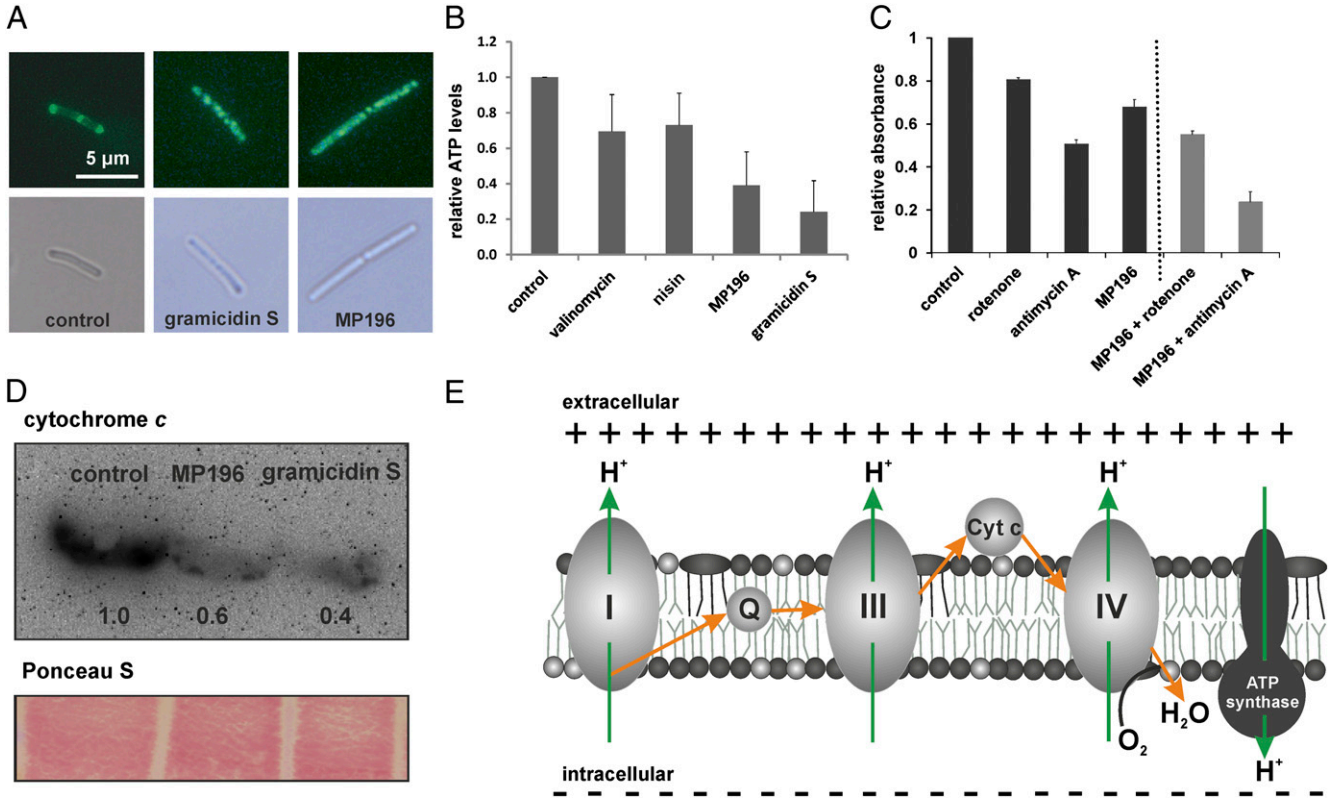

Fig. 4. Effects on membrane potential and respiration. (*A*) Fluorescence microscopy images (*Upper Row*) and corresponding bright-field images (*Lower Row*) show GFP-MinD localization in untreated *B. subtilis* cells and cells incubated with gramicidin S or MP196. GFP-MinD delocalization indicates membrane depolarization. (*B*) ATP levels of *B. subtilis* cells treated with valinomycin, nisin, gramicidin S, or MP196. In a luciferase assay, ATP concentrations were determined under conditions resembling those of the proteome experiment. (*C*) Activity of the respiratory chain of inverted *M. flavus* vesicles treated with rotenone, antimycin A, or MP196. Electron transport efficiency was monitored by the reduction of iodonitrotetrazolium chloride causing a decrease in absorbance at 485 nm. (*D*) Western analysis of cytochrome *c* in membrane fractions of *B. subtilis* after a 5-min treatment with gramicidin S and MP196. The Ponceau S-stained blot is displayed as loading control. (*E*) Overview of the bacterial respiratory chain [according to Vonck and Schäfer (38)]. Proton movements are indicated by green arrows; electron movements are indicated by orange arrows.

analysis of membrane fractions of antibiotic-treated *B. subtilis* cells (Fig. 4*D*). The amount of cytochrome *c* in the membrane was reduced drastically after 5 min of treatment with MP196, indicating dissociation of the protein from the extracellular membrane surface. This delocalization is independent of the membrane potential breaking down, because cytochrome *c* was detected in the membrane fraction of the untreated control cells, which were disrupted by ultrasonication. Rather, delocalization requires interaction of the peptide with the membrane. A similar effect was observed using gramicidin S, which previously was shown to inhibit components of the respiratory chain (37). Detachment of cytochrome *c* from the outer membrane leaflet explains the inhibition of the respiratory chain, breakdown of the membrane potential, and subsequent energy limitation (Fig. 4*E*) (38).

MP196 Undermines Cell-Wall Integrity by Delocalizing Another Essential Peripheral Membrane Protein. Following MP196 exposure, cell-wall biosynthesis is slightly inhibited (as revealed by precursor incorporation), severe cell-wall lesions form (as revealed by TEM), and there is a significant overlap of marker proteins with compounds that target membrane-bound steps of cell-wall biosynthesis in proteomic studies. When incorporation of cell-wall material is inhibited at a step in membrane-bound biosynthesis, *B. subtilis* cells undergo a characteristic change in shape after acetic acid/methanol fixation, namely extrusion of the cell membrane through holes in the cell wall (4, 26). Untreated cells and cells treated with valinomycin did not display membrane extrusions (Fig. 5*A*); nisin and MP196 did induce membrane extrusions, as did gramicidin S (although gramicidin S is not known to interfere directly with cell-wall biosynthesis).

A stereospecific target interaction was excluded by experiments with the D-MP196 variant. Therefore we investigated whether inhibition of a membrane-bound step of cell-wall biosynthesis could be attributed to the delocalization of a peripheral membrane protein, similar to the inhibition of the respiratory chain by cytochrome *c* delocalization. In *B. subtilis*, the only peripheral membrane protein in the pathway is MurG, the enzyme that converts lipid I to lipid II by attaching GlcNAc to the bactoprenol carrier-conjugated UDP-*N*-acetylmuramic acid (UDP-MurNAc) pentapeptide molecule. When the localization of MurG was investigated by Western blot analysis (Fig. 5*B*), both MP196 and gramicidin S treatment caused almost complete loss of MurG from the membrane fraction of treated *B. subtilis* within 5 min. The removal of MurG from the cytosolic membrane surface, in combination with energy limitation (see above), may explain the reduced glucosamine incorporation, loss of cell-wall integrity, and induction of a cell-wall–specific stress response. Inhibition of earlier cytosolic steps of cell-wall biosynthesis, inhibition of membrane-bound steps by lipid II binding, and direct inhibition of MurG activity were excluded experimentally (*SI Appendix, Results of Cell Wall Biosynthesis Inhibition Assays* and Fig. S7).

MP196 Integration Triggers MurG Release from Isolated *B. subtilis* Membranes. Western analysis of disrupted cell membranes revealed that both cytochrome *c* and MurG bind the membrane independent

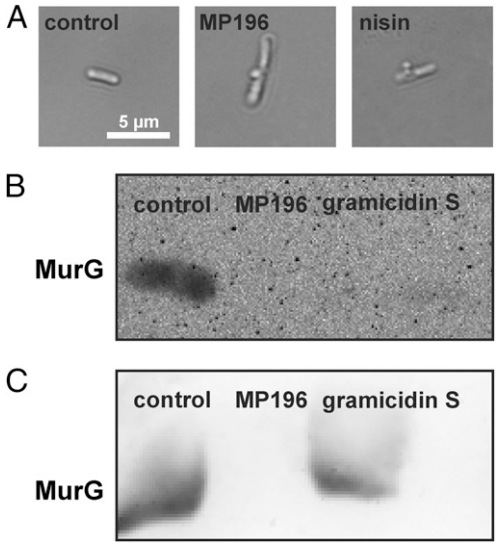

Fig. 5. Effects on the cell wall. (*A*) Light microscopy images showing cell-wall integrity of *B. subtilis* after treatment with MP196 and nisin. Acetic acid-methanol fixation visualizes cell-wall damage by extrusions of the membrane through holes in the cell wall. (*B*) Western blot detection of the cell-wall biosynthesis protein MurG in membrane fractions isolated from *B. subtilis* cells that were treated with peptide for 5 min. (*C*) Western blot detection of MurG in *B. subtilis* membrane fractions that first were isolated and then were incubated with peptide for 5 min.

of the membrane potential. To test if MP196 integration is sufficient for the release of MurG from the membrane, the membrane fraction of disrupted *B. subtilis* was collected and incubated with the peptide in vitro (Fig. 5*C*). Western blot analysis showed that MurG was released efficiently from the MP196-treated membrane fraction but remained attached to the untreated membrane, demonstrating that MP196 is sufficient for MurG detachment from the membrane.

***B. subtilis* Counteracts MP196 Action by Osmotic Stabilization.** Proteome analysis revealed up-regulation of proteins involved in amino acid anabolism, especially of glutamate and aspartate, within 65 min of MP196 treatment (*SI Appendix*, Table S3). To investigate the influence of MP196 on the amino acid pool, intracellular and extracellular free amino acid levels were measured by HPLC after 15 min of antibiotic treatment. MP196-treated cells accumulated free arginine and valine intracellularly (Fig. 6*A* and *SI Appendix*, Fig. S8*A*), consistent with the up-regulation of proteins involved in valine biosynthesis (*SI Appendix*, Table S3). Intracellular glutamine/glutamate, asparagine/aspartate (the assay used here does not distinguish between glutamate and glutamine or between aspartate and asparagine), lysine, and proline levels were substantially reduced, with concomitant dramatic increases in extracellular glutamine/glutamate and asparagine/aspartate and moderate increases in extracellular arginine, lysine, and proline (Fig. 6*B* and *SI Appendix*, Fig. S8*B*). The absolute amounts of glutamine/glutamate released exceeded by far the sum of intracellular and extracellular levels of untreated *B. subtilis* cultures, indicating dedicated biosynthesis and export (*SI Appendix*, Fig. S8*C*).

Supplementing defined medium with exogenous glutamate increased the MIC of MP196 against *B. subtilis* by up to eightfold (Fig. 6*C*), establishing that glutamate has a protective effect against MP196-induced stress. Similar results were obtained by supplementation with exogenous sodium chloride (Fig. 6*D*) and potassium chloride (Fig. 6*E*), suggesting that the protection against MP196 is not specific for glutamate but is caused by osmotic effects. Glutamate release also was observed in response to osmotic downshift and treatment with bacteriolytic peptides that target the membrane: the cyclic and cationic gramicidin S, the α-helical cationic aurein 2.2, the cationic lantibiotic nisin, or the uncharged amphiphilic gramicidin A. It was not observed after osmotic upshift or treatment with valinomycin or vancomycin, peptides that are either not bacteriolytic or do not target the membrane (Fig. 6*F*). Mechanosensitive channels appear to contribute to glutamate release after MP196 treatment. A *B. subtilis* mutant that lacks the four known MscL and MscS-type mechanosensitive channels (39) accumulated high levels of glutamate intracellularly (Fig. 6*G*) and showed heightened sensitivity to MP196 (Fig. 6 *C*–*E*). However, these channels are not the only route for glutamate release, because extracellular glutamate levels increased when the quadruple *msc* mutant was treated with MP196 (Fig. 6*B*).

Discussion

The cationic hexapeptide MP196, which is the minimal pharmacophore of RW-rich peptides, was used here to study the mechanism of action of short cationic antimicrobial peptides and subsequent bacterial adaptation strategies. MP196 acts on the bacterial cytoplasmic membrane (*SI Appendix*, Fig. S9 *A*, *I*), where essential physiological processes, including respiration (*SI Appendix*, Fig. S9 *A*, *II*), cell-wall biosynthesis (*SI Appendix*, Fig. S9 *A*, *III*), and membrane transport *SI Appendix*, Fig. S9 *A*, *IV*), take place. At the molecular level (*SI Appendix*, Fig. S9 *B*, *I*), MP196 integrates into the lipid bilayer readily and disturbs membrane architecture, as revealed by the perturbation of fatty acyl packing in the DSC analysis. This membrane integration likely is promoted by the interaction of the cationic arginine residues with negatively charged phospholipid head group and is facilitated by lipophilic tryptophan residues. Such a mechanism of membrane integration is typical of amphipathic peptides (13, 40–42), which accumulate in the membrane near the interface with the cytosol, making contact with lipid head groups and fatty acyl chains.

RW-rich peptides have been shown to differ in their ability to permeabilize membranes. Although the tridecapeptides tritrpticin and indolicidin permeabilize lipid bilayers (43), hexapeptides such as Combi-1 and Combi-2 showed very poor permeabilization (44). It is important to note that even peptides with very small structural differences can have distinct mechanisms of interacting with membranes, resulting in different permeabilization capabilities and modes of action, as shown recently for very small cyclic RW-rich peptides (45). Thus, the observations noted in this study may not necessarily apply to all antimicrobial peptides.

For MP196 we found no evidence for membrane permeabilization or pore formation in model membranes or in vivo. No ion release occurs in chemically defined bacterial culture medium. It has been suggested that integration of cationic amphiphatic peptides leads to local lipid reorganization and the formation of "peptide-induced lipid pores" that allow metal ions to cross the membrane (42); however, the lack of ion release in chemically defined medium suggests that ion efflux is not a major effect of MP196 under the growth conditions used in the proteome experiment.

The integration of MP196 into the membrane affects multiple cellular processes (*SI Appendix*, Fig. S9 *B*, *II–IV*). Like the RW-rich small cationic antimicrobial peptide Bac8c (46) and the small cyclic cationic peptide gramicidin S (37) that does not contain arginine or tryptophan residues, MP196 has a profound impact on the bacterial respiratory chain (*SI Appendix*, Fig. S9 *B*, *II*). Our data suggest that the inhibition of the respiratory chain by small cationic antimicrobial peptides is caused by the detachment of cytochrome *c* from the membrane, resulting in disruption of the electron transfer chain and subsequent breakdown of the proton gradient. Inhibition of the respiratory chain then affects ATP synthesis, causing energy limitation that impacts all other macromolecule biosynthesis pathways.

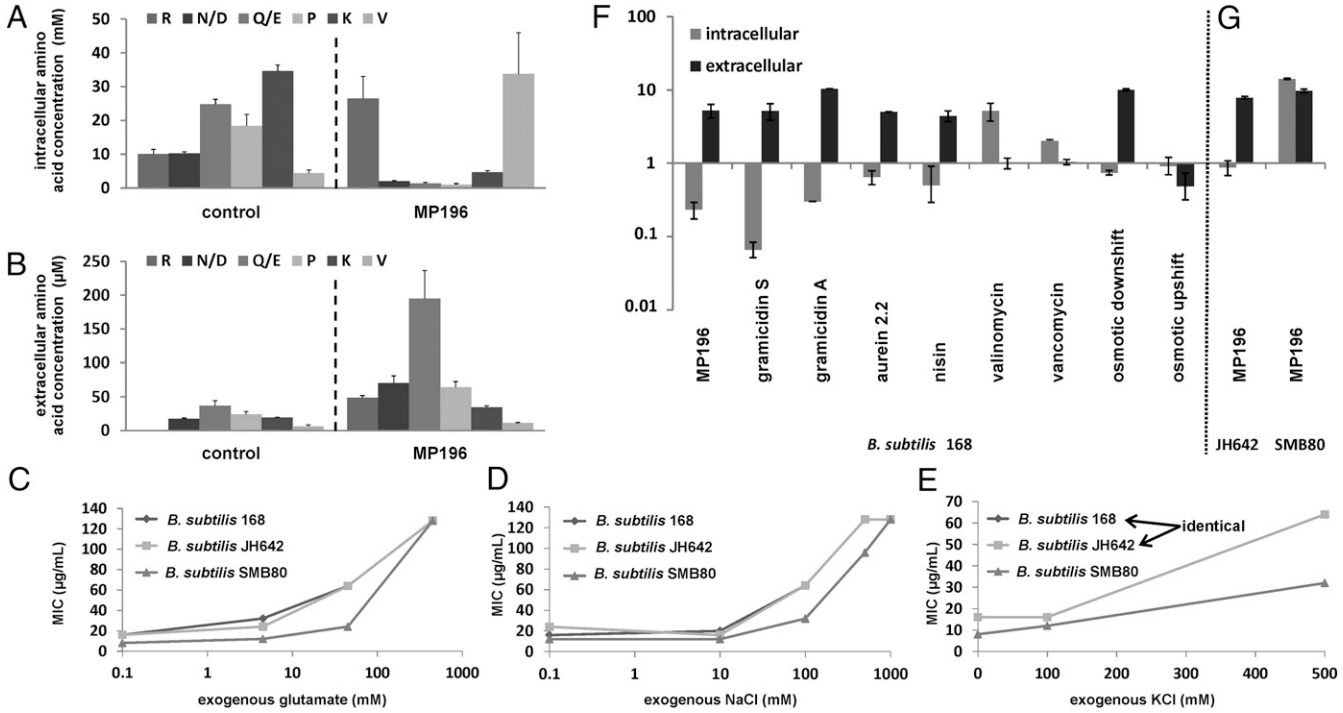

Fig. 6. Amino acid composition. (*A*) HPLC analysis of the intracellular amino acid composition of *B. subtilis* treated with MP196. (*B*) Extracellular amino acid composition of the same cultures. Only the amino acids whose concentrations changed significantly after peptide treatment are displayed here (see *SI Appendix*, Fig. S8 for full amino acid profiles). Amino acids are written in a one-letter code in the order of elution time from the column. Glutamate and glutamine as well as aspartate and asparagine are not distinguishable by this method and appear as one peak each. Tryptophan was not quantified here. (*C–E*) MICs of MP196 against *B. subtilis* 168, a *B. subtilis* strain lacking all known mechanosensitive channels (SMB80), and its parent strain (JH642) in defined medium supplemented with increasing glutamate (*C*), NaCl (*D*), or KCl (*E*) concentrations. MICs were determined independently twice. (*F*) Intra- and extracellular glutamate concentrations in *B. subtilis* cells under different antibiotic and osmotic stress conditions determined by amino acid analysis. (*G*) Intra- and extracellular glutamate concentrations in a *B. subtilis* JH642 and SMB80.

The impact of MP196 on cell-wall biosynthesis is illustrated by a reduction in precursor incorporation, promoter activation of cell-wall stress-responsive genes, up-regulation of proteins indicative of cell-wall biosynthesis stress, and loss of cell-wall integrity. Similar observations have been reported for gramicidin S (26) and Bac8c (46). In addition to an indirect effect on cell-wall biosynthesis caused by energy limitation, we found that small cationic peptides affect cell-wall biosynthesis by delocalizing the lipid II biosynthesis protein MurG from the intracellular surface of the membrane. As with cytochrome *c*, protein delocalization is independent of the membrane potential. Rather, it seems to be a consequence of the alterations in membrane architecture caused by peptide integration, which were observed by DSC. Delocalization of MurG could explain the effects on cell-wall biosynthesis and integrity exerted by MP196. This enzyme recently was shown to be the direct target of the anti-staphylococcal small molecule inhibitor murgocil (47).

We suggest that delocalization of peripheral membrane proteins is a general mechanism extending to membrane-targeting peptides of other structural classes such as the lipopeptide daptomycin. Daptomycin has been shown to alter membrane architecture and to delocalize the cell-division protein DivIVC, which binds the membrane in a curvature-dependent fashion (48–50). Although delocalization of MurG by daptomycin has not been described thus far, it would explain the induction of the cell-wall stress response (51).

A further consequence of MP196 treatment is the delocalization of the cell-division regulating protein, MinD. MinD previously was shown to delocalize upon membrane depolarization (35). MinD and MurG attach to the intracellular surface of the membrane through electrostatic interactions using an amphipathic helix motif (35, 52), whereas cytochrome *c* variants in *B. subtilis* attach to the outer leaflet of the membrane by a lipid anchor or transmembrane helices (53, 54). Thus, MP196 causes delocalization of proteins on both sides of the membrane, which attach to the membrane by different mechanisms. It is possible that, in addition to the proteins studied here, other membrane-associated proteins are delocalized as a consequence of MP196-mediated membrane injury.

Lacking evidence of a stereospecific binding site for MP196, no specific receptor–ligand interaction is apparent from our studies. In fact, our data suggest that the molecular target of MP196 is the lipid bilayer itself, and no other specific target than the membrane is identified. However, the main functional impact of MP196 is on proteins located in the membrane. Therefore MP196 interferes simultaneously with a broad range of cellular processes, complicating the development of bacterial resistance. DSC experiments showed that the interaction of MP196 with the membrane critically depends on lipid composition, thereby offering the opportunity to design peptides selective for Gram-positive and Gram-negative organisms over mammalian cells.

The proteome response and amino acid analysis provide evidence that *B. subtilis* counteracts peptide-mediated membrane stress by inducing three known defense strategies: adjustment of membrane lipid composition (55–57), stabilization of the membrane (58, 59), and restriction of access to the membrane by the enhancement of wall teichoic acid D-alanylation (*SI Appendix*, Fig. S9 *C*, *I–III*; see *SI Appendix* for details) (31, 60–62). Here we describe another survival strategy, one that entails the release of selected amino acids from the cells (*SI Appendix*, Fig. S9 *C*, *IV*). Large quantities of glutamine/glutamate, plus significant amounts of asparagine/aspartate, arginine, proline, and lysine, were released

into the medium, and biosynthesis of these amino acids was reflected in the proteome response.

The release of amino acids is mediated in part by mechanosensitive channels, which measure membrane tension, and their transient opening is triggered by turgor-induced pressure on the lipid bilayer (63). In plants, the activation of host defense by bacterial antimicrobial peptides has been attributed to mechanoreceptors directly sensing peptide-induced alterations in membrane architecture (64–66).

Glutamate is an osmoprotectant that accumulates intracellularly in some bacilli. In *B. subtilis* it is the most abundant free amino acid, with a pool size of about 100 mM (67).

Under hyperosmotic stress the intracellular glutamate pool increases moderately (up to about 170 mM) (67). Under these conditions the outflow of water is prevented by increasing proline levels (depending on the severity of the environmentally imposed osmotic stress) up to pool sizes of 500 mM in severely stressed cells (68–70). Upon osmotic downshock the opposite is the case: *Escherichia coli* releases potassium glutamate into the medium using mechanosensitive channels (71). In *Corynebacterium glutamicum* glutamate excretion through mechanosensitive channels is triggered in response to penicillin treatment (72). We show here that *B. subtilis* also releases glutamate in response to hypoosmotic stress conditions. Glutamate release is triggered further in response to treatment with membrane-targeting bacteriolytic peptides belonging to different structural classes (cyclodecapeptide gramicidin S, α-helical amphiphile aurein 2.2, lantibiotic nisin, and uncharged amphiphilic gramicidin A) (Fig. 6*F*). These results suggest that osmoprotective glutamate release is a general reaction to membrane-targeting bacteriolytic peptides. The addition of exogenous glutamate to the growth medium protected against MP196 via osmotic stabilization (Fig. 6 *C*–*E*). Similar observations were made for sublancin 168, a glycopeptide with an unknown mechanism of action produced by *B. subtilis* 168. High NaCl concentrations lowered the susceptibility of sublancin-sensitive strains (73). High salt concentrations also negatively affected the susceptibility of *S. aureus* strains to the human antimicrobial peptides LL-37 (α-helical) and HNP-1 (β-sheet defensin) (74) as well as to the bactericidal activity of the small cationic peptide thrombin-induced platelet microbicidal protein tPMP (75).

This report provides a detailed physiological study of the in vivo mechanism of action of a short RW-rich antimicrobial peptide, which we chose as a model to study the action of short cationic antimicrobial peptides. It illustrates how MP196 integrates into the membrane, leading to delocalization of peripheral membrane proteins. This delocalization includes the detachment of the essential proteins cytochrome *c* and MurG from the cytoplasmic membrane, impacting energy metabolism and cell-wall biosynthesis. We propose that substantial energy limitation and loss of cell-wall integrity resulting from the delocalization of essential peripheral membrane proteins are the major factors that contribute to MP196-mediated bacterial cell death. These perspectives on the action of small cationic antimicrobial peptides, involving lipids and proteins, are complementary to the lipid-focused pore formation and carpet mechanism models. Based on the data presented here, we suggest that MP196 action follows the interfacial activity model described by Wimley and Hristova (11), whereby, at a reduction in growth rate of 50%, phospholipid perturbation predominates over membrane disruption.

We also describe a bacterial defense strategy against bacteriolytic membrane-targeting peptides that relies on lowering the considerable osmotic potential of the *B. subtilis* cell, and hence the magnitude of turgor (67), through the release of selected amino acids into the medium.

Materials and Methods

Experimental details and citations for all methods are provided in *SI Appendix*.

Radioactive Precursor Incorporation. The influence of MP196 on the major macromolecular synthesis routes was studied by incorporation of radioactively labeled precursor molecules by *Staphylococcus simulans* as described by Schneider et al. (76).

Reporter Gene Activation. Damage to the main cellular macromolecules was monitored by promoter activation of selected marker genes fused to the firefly luciferase reporter gene in the genetic background of *B. subtilis* IS34. Serial twofold dilutions of each peptide (0.031–64 μg/mL) were inoculated with bacterial cell suspensions and incubated at 37 °C for a time period depending on the induction kinetics of the reporter strain. Then 2 mM luciferin was added, and flash luminescence was measured.

Proteomics. Treatment of *B. subtilis* 168, metabolic labeling of newly synthesized proteins with [^{35}S]-L-methionine, and subsequent protein separation by 2D PAGE were performed as described previously (25). For gel-free proteome analysis of membrane proteins, *B. subtilis* 168 was grown aerobically at 37 °C in Belitzky minimal medium (BMM) supplemented with ^{14}*N*-ammonium sulfate and ^{14}*N*-L-tryptophan. Cells were stressed at an OD_{500} of 0.4 with 22.5 μg/mL MP196 for 65 min or were left untreated as control. Untreated cultures grown on ^{15}*N*-ammonium sulfate and ^{15}*N*-L-tryptophan were used for relative quantification. Mixing of cell extracts before subcellular fractionation steps for relative quantification was carried out according to Otto et al. (77). The enriched membrane protein fraction was prepared according to the workflow published by Eymann et al. (78), omitting the n-dodecyl-β-D-maltoside treatment step. The preparation of the integral membrane peptides was carried out as described by Wolff et al. (79). Sample preparation, mass spectrometric measurement, and subsequent data analysis were carried out as described by Otto et al. (77). The mass spectrometry proteomics data have been deposited with the ProteomeXchange Consortium (http://proteomecentral.proteomexchange.org) via the PRIDE partner repository (80) with the dataset identifier PXD000181.

TEM. Cells were grown in BMM to an OD_{500} of 0.35. The main culture then was subdivided into 50-mL aliquots, and subcultures were treated with the respective antibiotics for 15 min or were left untreated as control. Cells were harvested by centrifugation and washed twice in 100 mM Tris/1 mM EDTA, pH 7.5, and subsequently were washed once in the same buffer without EDTA. Bacterial samples for TEM were prepared according to Santhana Raj et al. (81) with some modifications (see *SI Appendix, Experimental Details*). To study effects on the cell envelope, sections were stained with 0.2% lead citrate in 0.1 M NaOH for 3 s. Samples were examined at 23,000–230,000× magnification with a Philips EM410 transmission electron microscope equipped with a Gatan digital camera system at an accelerating voltage of 80 kV.

For peptide tracing, cell cultures were treated with 1 μg/mL of the ruthenocene-substituted MP196 derivative MP276 (*SI Appendix*, Fig. S3*D*) for 15 min before sample preparation for TEM. The lead-staining step was omitted.

Graphite Furnace Atomic Absorption Spectrometry. Cytosolic, membrane, and cell-wall fractions of untreated and MP276-treated *B. subtilis* were prepared. To this end, cells were harvested and washed five times with 100 mM Tris/1 mM EDTA before ultrasonication, centrifugation, and ultracentrifugation. Ruthenium contents were quantified using a Vario 6 graphite furnace atomic absorption spectrometer (Analytik Jena) as described previously (82–84).

Differential Scanning Calorimetry. Membrane integration was investigated by DSC-based determination of peptide-induced changes in the thermotropic-phase behavior of liposomes consisting of pure DPPG, pure DPPE, pure DPPC, and a mixture of 88% DPPG and 12% DPPE, respectively.

Permeability Assays. In vivo pore formation in *B. subtilis 168* was monitored using the Live/Dead BacLight bacterial viability kit (Invitrogen) following the manufacturer's instructions. Potassium release from *B. megaterium* was performed as described previously (26).

Global Ion Analysis. Ionomics experiments were performed with *B. subtilis* 168 in minimal medium under the same conditions as the proteomics experiments. Ion concentrations were determined by inductively coupled plasma atomic emission spectroscopy.

Membrane Potential Measurements. GFP-MinD localization assays were performed with *B. subtilis* 1981 GFP-MinD (35) as described previously (26).

Determination of membrane potential changes by use of $DiSC_35$ was performed as described by Andrés and Fierro (36) in *B. megaterium*.

ATP Assay. ATP concentrations were determined from *B. subtilis* cytosolic extracts using the Perkin-Elmer ATPlite 1 step assay according to the manufacturer's instructions.

ATPase and Respiratory Chain Assays. *M. flavus* inverted vesicles for H^+-ATPase and respiratory chain activity measurements were prepared according to Burstein et al. (85). Proton pumping into *M. flavus* inverted vesicles by H^+-ATPase was measured in a microtiter plate assay based on the pH-sensitive probe acridine orange as described by Palmgren et al. (86). Antibiotic influence on the bacterial electron transport chain was monitored by reduction of iodonitrotetrazolium chloride using *M. flavus* inverted vesicles as described by Smith and McFeters (87). Cytochrome *c* localization was determined by Western blot detection of cytochrome *c* on the same blots used for MurG detection.

Cell-Wall Integrity and Inhibition of Biosynthesis. Sample preparation and bright field microscopic inspection of *B. subtilis* 168 was performed as described previously (26).

To detect MurG in membrane fractions of *B. subtilis* 168, cells were grown in BMM until early logarithmic growth phase, treated with antibiotics for 5 min, and harvested by centrifugation. Membrane fractions were separated by differential centrifugation, subjected to SDS PAGE, and blotted onto a nitrocellulose membrane. MurG was detected with an *E. coli* MurG-specific antibody produced in rabbit and a secondary goat anti-rabbit IgG-HRP conjugate (BioRad).

Inhibition of in vitro lipid II synthesis was performed using *M. flavus* DSM 1790 membrane preparations as described by Schneider et al. (76). For in vitro lipid II binding, peptides were incubated with 2 nmol lipid II in 1:1 molar ratios. Reaction mixtures were incubated at 30 °C for 30 min and applied onto TLC plates (TLC Silica Gel 60 F_{254}; Merck). Chromatography was performed in chloroform-methanol-water-ammonia (88:48:10:1) and stained with phosphomolybdic acid stain at 140 °C. Accumulation of UPP-MurNac pentapeptide was analyzed by HPLC as described by Schmitt et al. (88).

Amino Acid Analysis. Amino acid analysis of *B. subtilis* 168 (*trpC2*), *B. subtilis* JH642 (*trpC2 pheA1*), and SMB80 (*trpC2 pheA1 mscL yhdY ykuT yfkC*) (41) cellular extracts and culture supernatants was performed by HPLC using the Acquity HPLC and AccQ•Tag Ultra system (Waters GmbH) according to the manufacturer's instructions. Before HPLC, proteins were removed by acetone precipitation.

MIC values against *B. subtilis* strains were determined with 5×10^5 cells/mL in BMM supplemented with increasing concentrations of glutamate, sodium chloride, or potassium chloride. The lowest concentration inhibiting visible growth was taken as the MIC.

ACKNOWLEDGMENTS. We thank Michaele Josten, Petra Düchting, Monika Bürger and Beate Menzel, and Stephanie Tautges, Kathrin Barlog, and Jale Stoutjesdijk for excellent technical assistance; Christoph H. R. Senges for help in preparing *B. subtilis* samples; Sina Langklotz and Dirk Albrecht for assistance with mass spectrometry; Helmut Meyer for providing amino acid analysis technology; Klaus Funke and Ellen Kloosterboer for providing the cytochrome *c* antibody; Tanneke de Blaauwen and Franz Naberhaus for providing the MurG antibody; and AiCuris, GmbH for providing the *B. subtilis* reporter strains. This manuscript was written in part at the 2013 Scientific Writing workshop of the Ruhr University Bochum (RUB) Research School; we thank Lars Leichert and Richard Gallagher for critically reading the manuscript and for many helpful suggestions. This work was supported by a grant from the German federal state of North Rhine-Westphalia and the European Union (European Regional Development Fund "Investing in your future") (to N.M.-N., H.B.-O., H.-G.S., and J.E.B.) and by the RUB Research Department Interfacial Systems Chemistry (N.M.-N. and J.E.B.). C.M. was supported by the Protein Unit for Research in Europe, a project of North Rhine-Westphalia.

1. Giuliani A, Pirri G, Nicoletto SF (2007) Antimicrobial peptides: An overview of a promising class of therapeutics. *Cent Eur J Biol* 2(1):1–33.
2. Riedl S, Zweytick D, Lohner K (2011) Membrane-active host defense peptides—challenges and perspectives for the development of novel anticancer drugs. *Chem Phys Lipids* 164(8):766–781.
3. Mygind PH, et al. (2005) Plectasin is a peptide antibiotic with therapeutic potential from a saprophytic fungus. *Nature* 437(7061):975–980.
4. Schneider T, et al. (2010) Plectasin, a fungal defensin, targets the bacterial cell wall precursor Lipid II. *Science* 328(5982):1168–1172.
5. Patra M, Gasser G, Metzler-Nolte N (2012) Small organometallic compounds as antibacterial agents. *Dalton Trans* 41(21):6350–6358.
6. Pag U, et al. (2008) Analysis of *in vitro* activities and modes of action of synthetic antimicrobial peptides derived from an alpha-helical 'sequence template'. *J Antimicrob Chemother* 61(2):341–352.
7. Zelezetsky I, Tossi A (2006) Alpha-helical antimicrobial peptides—using a sequence template to guide structure-activity relationship studies. *Biochim Biophys Acta* 1758(9):1436–1449.
8. Zelezetsky I, et al. (2005) Controlled alteration of the shape and conformational stability of alpha-helical cell-lytic peptides: Effect on mode of action and cell specificity. *Biochem J* 390(Pt 1):177–188.
9. Rathinakumar R, Walkenhorst WF, Wimley WC (2009) Broad-spectrum antimicrobial peptides by rational combinatorial design and high-throughput screening: The importance of interfacial activity. *J Am Chem Soc* 131(22):7609–7617.
10. Sharma RK, Sundriyal S, Wangoo N, Tegge W, Jain R (2010) New antimicrobial hexapeptides: Synthesis, antimicrobial activities, cytotoxicity, and mechanistic studies. *ChemMedChem* 5(1):86–95.
11. Wimley WC, Hristova K (2011) Antimicrobial peptides: Successes, challenges and unanswered questions. *J Membr Biol* 239(1-2):27–34.
12. Yeaman MR, Yount NY (2003) Mechanisms of antimicrobial peptide action and resistance. *Pharmacol Rev* 55(1):27–55.
13. Chan DI, Prenner EJ, Vogel HJ (2006) Tryptophan- and arginine-rich antimicrobial peptides: Structures and mechanisms of action. *Biochim Biophys Acta* 1758(9): 1184–1202.
14. Zweytick D, et al. (2011) Studies on lactoferricin-derived *Escherichia coli* membrane-active peptides reveal differences in the mechanism of N-acylated versus nonacylated peptides. *J Biol Chem* 286(24):21266–21276.
15. Zweytick D, Tumer S, Blondelle SE, Lohner K (2008) Membrane curvature stress and antibacterial activity of lactoferricin derivatives. *Biochem Biophys Res Commun* 369(2):395–400.
16. Chantson JT, Verga Falzacappa MV, Crovella S, Metzler-Nolte N (2006) Solid-phase synthesis, characterization, and antibacterial activities of metallocene-peptide bioconjugates. *ChemMedChem* 1(11):1268–1274.
17. Strøm MB, et al. (2003) The pharmacophore of short cationic antibacterial peptides. *J Med Chem* 46(9):1567–1570.
18. Albada HB, et al. (2012) Modulating the activity of short arginine-tryptophan containing antibacterial peptides with N-terminal metallocenoyl groups. *Beilstein J Org Chem* 8:1753–1764.
19. Albada HB, et al. (2012) Tuning the activity of short Arg-Trp antimicrobial peptides by lipidation of C- or N-terminal lysine side-chain. *ACS Med Chem Lett* 3(12):980–984.
20. Albada HB, et al. (2013) Short antibacterial peptides with significantly reduced hemolytic activity can be identified by a systematic L-to-D exchange scan of their amino acid residues. *ACS Comb Sci* 15(11):585–592.
21. Urban A, et al. (2007) Novel whole-cell antibiotic biosensors for compound discovery. *Appl Environ Microbiol* 73(20):6436–6443.
22. Brötz-Oesterhelt H, et al. (2005) Dysregulation of bacterial proteolytic machinery by a new class of antibiotics. *Nat Med* 11(10):1082–1087.
23. Bandow JE (2005) Proteomic approaches to antibiotic drug discovery. *Curr Protoc Microbiol* Chapter 1:2.
24. Bandow JE, Brötz H, Leichert LI, Labischinski H, Hecker M (2003) Proteomic approach to understanding antibiotic action. *Antimicrob Agents Chemother* 47(3):948–955.
25. Wenzel M, et al. (2011) Proteomic signature of fatty acid biosynthesis inhibition available for in vivo mechanism-of-action studies. *Antimicrob Agents Chemother* 55(6):2590–2596.
26. Wenzel M, et al. (2012) Proteomic response of *Bacillus subtilis* to lantibiotics reflects differences in interaction with the cytoplasmic membrane. *Antimicrob Agents Chemother* 56(11):5749–5757.
27. Katsu T, et al. (1989) Mechanism of membrane damage induced by the amphipathic peptides gramicidin S and melittin. *Biochim Biophys Acta* 983(2):135–141.
28. Gross A, et al. (2012) A ruthenocene-PNA bioconjugate—synthesis, characterization, cytotoxicity, and AAS-detected cellular uptake. *Bioconjug Chem* 23(9):1764–1774.
29. Matias VR, Beveridge TJ (2005) Cryo-electron microscopy reveals native polymeric cell wall structure in *Bacillus subtilis* 168 and the existence of a periplasmic space. *Mol Microbiol* 56(1):240–251.
30. Matias VR, Beveridge TJ (2008) Lipoteichoic acid is a major component of the *Bacillus subtilis* periplasm. *J Bacteriol* 190(22):7414–7418.
31. Weidenmaier C, Peschel A (2008) Teichoic acids and related cell-wall glycopolymers in Gram-positive physiology and host interactions. *Nat Rev Microbiol* 6(4):276–287.
32. Clejan S, Krulwich TA, Mondrus KR, Seto-Young D (1986) Membrane lipid composition of obligately and facultatively alkalophilic strains of *Bacillus spp*. *J Bacteriol* 168(1):334–340.
33. Brisebois PP, Arnold AA, Chabre YM, Roy R, Marcotte I (2012) Comparative study of the interaction of fullerenol nanoparticles with eukaryotic and bacterial model membranes using solid-state NMR and FTIR spectroscopy. *Eur Biophys J* 41(6):535–544.
34. Duax WL, et al. (1996) Molecular structure and mechanisms of action of cyclic and linear ion transport antibiotics. *Biopolymers* 40(1):141–155.
35. Strahl H, Hamoen LW (2010) Membrane potential is important for bacterial cell division. *Proc Natl Acad Sci USA* 107(27):12281–12286.
36. Andrés MT, Fierro JF (2010) Antimicrobial mechanism of action of transferrins: Selective inhibition of H^+-ATPase. *Antimicrob Agents Chemother* 54(10):4335–4342.

37. Mogi T, Ui H, Shiomi K, Omura S, Kita K (2008) Gramicidin S identified as a potent inhibitor for cytochrome *bd*-type quinol oxidase. *FEBS Lett* 582(15):2299–2302.
38. Vonck J, Schäfer E (2009) Supramolecular organization of protein complexes in the mitochondrial inner membrane. *Biochim Biophys Acta* 1793(1):117–124.
39. Hoffmann T, Boiangiu C, Moses S, Bremer E (2008) Responses of *Bacillus subtilis* to hypotonic challenges: Physiological contributions of mechanosensitive channels to cellular survival. *Appl Environ Microbiol* 74(8):2454–2460.
40. Sitaram N, Nagaraj R (1999) Interaction of antimicrobial peptides with biological and model membranes: Structural and charge requirements for activity. *Biochim Biophys Acta* 1462(1-2):29–54.
41. Epand RM, et al. (2010) Lipid clustering by three homologous arginine-rich antimicrobial peptides is insensitive to amino acid arrangement and induced secondary structure. *Biochim Biophys Acta* 1798(6):1272–1280.
42. Fuertes G, Giménez D, Esteban-Martín S, Sánchez-Muñoz OL, Salgado J (2011) A lipocentric view of peptide-induced pores. *Eur Biophys J* 40(4):399–415.
43. Schibli DJ, Epand RF, Vogel HJ, Epand RM (2002) Tryptophan-rich antimicrobial peptides: Comparative properties and membrane interactions. *Biochem Cell Biol* 80(5):667–677.
44. Rezansoff AJ, et al. (2005) Interactions of the antimicrobial peptide Ac-FRWWHR-$NH(_2)$ with model membrane systems and bacterial cells. *J Pept Res* 65(5):491–501.
45. Scheinpflug K, Nikolenko H, Komarov IV, Rautenbach M, Dathe M (2013) What goes around comes around-a comparative study of the influence of chemical modifications on the antimicrobial properties of small cyclic peptides. *Pharmaceuticals (Basel)* 6(9): 1130–1144.
46. Spindler EC, Hale JD, Giddings TH, Jr., Hancock RE, Gill RT (2011) Deciphering the mode of action of the synthetic antimicrobial peptide Bac8c. *Antimicrob Agents Chemother* 55(4):1706–1716.
47. Mann PA, et al. (2013) Murgocil is a highly bioactive staphylococcal-specific inhibitor of the peptidoglycan glycosyltransferase enzyme MurG. *ACS Chem Biol* 8(11):2442–2451.
48. Pogliano J, Pogliano N, Silverman JA (2012) Daptomycin-mediated reorganization of membrane architecture causes mislocalization of essential cell division proteins. *J Bacteriol* 194(17):4494–4504.
49. Bayer AS, Schneider T, Sahl H-G (2013) Mechanisms of daptomycin resistance in *Staphylococcus aureus*: Role of the cell membrane and cell wall. *Ann N Y Acad Sci* 1277:139–158.
50. Lenarcic R, et al. (2009) Localisation of DivIVA by targeting to negatively curved membranes. *EMBO J* 28(15):2272–2282.
51. Wecke T, et al. (2009) Daptomycin versus Friulimicin B: In-depth profiling of *Bacillus subtilis* cell envelope stress responses. *Antimicrob Agents Chemother* 53(4):1619–1623.
52. Ha S, Walker D, Shi Y, Walker S (2000) The 1.9 A crystal structure of *Escherichia coli* MurG, a membrane-associated glycosyltransferase involved in peptidoglycan biosynthesis. *Protein Sci* 9(6):1045–1052.
53. Bengtsson J, Tjalsma H, Rivolta C, Hederstedt L (1999) Subunit II of *Bacillus subtilis* cytochrome *c* oxidase is a lipoprotein. *J Bacteriol* 181(2):685–688.
54. Bengtsson J, Rivolta C, Hederstedt L, Karamata D (1999) *Bacillus subtilis* contains two small *c*-type cytochromes with homologous heme domains but different types of membrane anchors. *J Biol Chem* 274(37):26179–26184.
55. Fränzel B, et al. (2010) *Corynebacterium glutamicum* exhibits a membrane-related response to a small ferrocene-conjugated antimicrobial peptide. *J Biol Inorg Chem* 15(8):1293–1303.
56. López D, Kolter R (2010) Functional microdomains in bacterial membranes. *Genes Dev* 24(17):1893–1902.
57. Kingston AW, Subramanian C, Rock CO, Helmann JD (2011) A σ^W-dependent stress response in *Bacillus subtilis* that reduces membrane fluidity. *Mol Microbiol* 81(1): 69–79.
58. Wolf D, et al. (2010) In-depth profiling of the LiaR response of Bacillus subtilis. *J Bacteriol* 192(18):4680–4693.
59. Kobayashi R, Suzuki T, Yoshida M (2007) *Escherichia coli* phage-shock protein A (PspA) binds to membrane phospholipids and repairs proton leakage of the damaged membranes. *Mol Microbiol* 66(1):100–109.
60. Bertsche U, et al. (2011) Correlation of daptomycin resistance in a clinical *Staphylococcus aureus* strain with increased cell wall teichoic acid production and D-alanylation. *Antimicrob Agents Chemother* 55(8):3922–3928.
61. Rose WE, Fallon M, Moran JJ, Vanderloo JP (2012) Vancomycin tolerance in methicillin-resistant *Staphylococcus aureus*: Influence of vancomycin, daptomycin, and telavancin on differential resistance gene expression. *Antimicrob Agents Chemother* 56(8):4422–4427.
62. Saar-Dover R, et al. (2012) D-alanylation of lipoteichoic acids confers resistance to cationic peptides in group B *streptococcus* by increasing the cell wall density. *PLoS Pathog* 8(9):e1002891.
63. Booth IR, Blount P (2012) The MscS and MscL families of mechanosensitive channels act as microbial emergency release valves. *J Bacteriol* 194(18):4802–4809.
64. Henry G, Deleu M, Jourdan E, Thonart P, Ongena M (2011) The bacterial lipopeptide surfactin targets the lipid fraction of the plant plasma membrane to trigger immune-related defence responses. *Cell Microbiol* 13(11):1824–1837.
65. Desoignies N, Schramme F, Ongena M, Legrève A (2013) Systemic resistance induced by *Bacillus* lipopeptides in *Beta vulgaris* reduces infection by the rhizomania disease vector *Polymyxa betae*. *Mol Plant Pathol* 14(4):416–421.
66. Brotman Y, Makovitzki A, Shai Y, Chet I, Viterbo A (2009) Synthetic ultrashort cationic lipopeptides induce systemic plant defense responses against bacterial and fungal pathogens. *Appl Environ Microbiol* 75(16):5373–5379.
67. Whatmore AM, Chudek JA, Reed RH (1990) The effects of osmotic upshock on the intracellular solute pools of *Bacillus subtilis*. *J Gen Microbiol* 136(12):2527–2535.
68. Hoffmann T, et al. (2012) Synthesis, release, and recapture of compatible solute proline by osmotically stressed Bacillus subtilis cells. *Appl Environ Microbiol* 78(16): 5753–5762.
69. Hoffmann T, et al. (2013) Osmotic control of *opuA* expression in *Bacillus subtilis* and its modulation in response to intracellular glycine betaine and proline pools. *J Bacteriol* 195(3):510–522.
70. Zaprasis A, et al. (2013) Osmoprotection of *Bacillus subtilis* through import and proteolysis of proline-containing peptides. *Appl Environ Microbiol* 79(2):576–587.
71. Ajouz B, Berrier C, Garrigues A, Besnard M, Ghazi A (1998) Release of thioredoxin via the mechanosensitive channel MscL during osmotic downshock of *Escherichia coli* cells. *J Biol Chem* 273(41):26670–26674.
72. Becker M, et al. (2013) Glutamate efflux mediated by *Corynebacterium glutamicum* MscCG, *Escherichia coli* MscS, and their derivatives. *Biochim Biophys Acta* 1828(4): 1230–1240.
73. Kouwen TR, et al. (2009) The large mechanosensitive channel MscL determines bacterial susceptibility to the bacteriocin sublancin 168. *Antimicrob Agents Chemother* 53(11):4702–4711.
74. Turner J, Cho Y, Dinh NN, Waring AJ, Lehrer RI (1998) Activities of LL-37, a cathelin-associated antimicrobial peptide of human neutrophils. *Antimicrob Agents Chemother* 42(9):2206–2214.
75. Koo SP, Yeaman MR, Bayer AS (1996) Staphylocidal action of thrombin-induced platelet microbicidal protein is influenced by microenvironment and target cell growth phase. *Infect Immun* 64(9):3758–3764.
76. Schneider T, et al. (2004) *In vitro* assembly of a complete, pentaglycine interpeptide bridge containing cell wall precursor (lipid II-Gly5) of *Staphylococcus aureus*. *Mol Microbiol* 53(2):675–685.
77. Otto A, et al. (2010) Systems-wide temporal proteomic profiling in glucose-starved *Bacillus subtilis*. *Nat Commun* 1:137.
78. Eymann C, et al. (2004) A comprehensive proteome map of growing *Bacillus subtilis* cells. *Proteomics* 4(10):2849–2876.
79. Wolff S, Hahne H, Hecker M, Becher D (2008) Complementary analysis of the vegetative membrane proteome of the human pathogen *Staphylococcus aureus*. *Mol Cell Proteomics* 7(8):1460–1468.
80. Vizcaíno JA, et al. (2013) The PRoteomics IDEntifications (PRIDE) database and associated tools: Status in 2013. *Nucleic Acids Res* 41(Database issue):D1063–D1069.
81. Santhana Raj L, et al. (2007) Rapid method for transmission electron microscopy study of *Staphylococcus aureus* ATCC 25923. *Annals of Microscopy* 7:102–108.
82. Gust R, et al. (1998) Stability and cellular studies of [*rac*-1,2-bis(4-fluorophenyl)-ethylenediamine][cyclobutane-1,1- dicarboxylato]platinum(II), a novel, highly active carboplatin derivative. *J Cancer Res Clin Oncol* 124(11):585–597.
83. Schäfer S, Ott I, Gust R, Sheldrick WS (2007) Influence of the polypyridyl (pp) ligand size on the DNA binding properties, cytotoxicity and cellular uptake of organoruthenium(II) complexes of the type $[(\eta^6\text{-}C_6Me_6)Ru(L)(pp)]^{n+}$. *Eur J Inorg Chem* 19:3034–3046.
84. Schatzschneider U, et al. (2008) Cellular uptake, cytotoxicity, and metabolic profiling of human cancer cells treated with ruthenium(II) polypyridyl complexes [Ru(bpy)2 (N—N)]Cl2 with N—N=bpy, phen, dpq, dppz, and dppn. *ChemMedChem* 3(7): 1104–1109.
85. Burstein C, Tiankova L, Kepes A (1979) Respiratory control in *Escherichia coli* K 12. *Eur J Biochem* 94(2):387–392.
86. Palmgren MG, Sommarin M, Ulvskov P, Larsson C (1990) Effect of detergents on the $H^{(+)}$-ATPase activity of inside-out and right-side-out plant plasma membrane vesicles. *Biochim Biophys Acta* 1021(2):133–140.
87. Smith JJ, McFeters GA (1997) Mechanisms of INT (2-(4-iodophenyl)-3-(4-nitrophenyl)-5-phenyl tetrazolium chloride), and CTC (5-cyano-2,3-ditolyl tetrazolium chloride) reduction in *Escherichia coli* K-12. *J Microbiol Methods* 29(1):161–175.
88. Schmitt P, et al. (2010) Insight into invertebrate defensin mechanism of action: Iyster defensins inhibit peptidoglycan biosynthesis by binding to lipid II. *J Biol Chem* 285(38):29208–29216.